JCTC Journal of Chemical Theory and Computation

pubs.acs.org/JCTC Article

First-Principles Simulations of X-ray Transient Absorption for Probing Attosecond Electron Dynamics

Min Chen and Kenneth Lopata*

Cite This: J. Chem. Theory Comput. 2020, 16, 4470−4478 Read Online

ACCESS | Metrics & More | Article Recommendations | Supporting Information

ABSTRACT: X-ray transient absorption spectroscopy (XTAS) is a promising technique for measuring electron dynamics in molecules and solids with attosecond time resolutions. In XTAS, the elemental specificity and spatial locality of core-to-valence X-ray absorption is exploited to relate modulations in the time-resolved absorption spectra to local electron density variations around particular atoms. However, interpreting these absorption modulations and frequency shifts as a function of the time delay in terms of dynamics can be challenging. In this paper, we present a first-principles study of attosecond XTAS in a selection of simple molecules based on real-time time-dependent density functional theory (RT-TDDFT) with constrained DFT to emulate the state of the system following the interaction with a ultraviolet pump laser. In general, there is a decrease in the optical density and a blue shift in the frequency with increasing electron density around the absorbing atom. In carbon monoxide (CO), modulations in the O K-edge occur at the frequency of the valence electron dynamics, while for dioxygen (O_2) they occur at twice the frequency, due to the indistinguishability of the oxygen atoms. In 4-aminophenol ($H_2NC_6H_4OH$), likewise, there is a decrease in the optical density and a blue shift in the frequency for the oxygen and nitrogen K-edges with increasing charge density on the O and N, respectively. Similar effects are observed in the nitrogen K-edge for a long-range charge-transfer excitation in a benzene (C_6H_6)−tetracyanoethylene (C_6N_4; TCNE) dimer but with weaker modulations due to the delocalization of the charge across the entire TCNE molecule. Additionally, in all cases, there are pre-edge features corresponding to core transitions to depopulated orbitals. These potentially offer a background-free signal that only appears in pumped molecules.

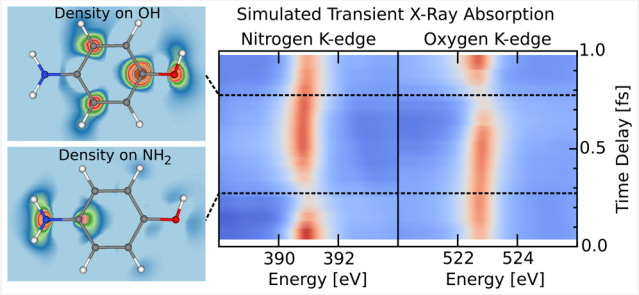

1. INTRODUCTION

Measuring subfemtosecond electron dynamics in molecules and materials has been the focus of much recent interest. These dynamics, which result from a coherent superposition of states, occur at time scales faster than nuclear motion.[1−8] These dynamics form the initial stages of photochemical and light-harvesting processes, which are still poorly understood. In solids, electron dynamics resulting from intense laser pulses result in band dynamics such as band distortion and valence band/conduction band redistribution[9−11] and result in strong-field effects like negative-differential conductivity.[12] Understanding these transformations is critically important for predicting and tuning optical breakdown, such as for high density circuitry and energy storage. Molecular and solid-state attosecond experiments are poised to shed light on these processes, but progress hinges on developing methods capable of measuring electron density changes with attosecond time resolutions.

There have been numerous approaches[13,14] developed to measure electron dynamics, including high-harmonic spectroscopy (HHS),[15,16] time-resolved photoemission spectroscopy,[17] attosecond streaking,[18] wave packet interferometry,[19] attosecond transient absorption (ATA),[11,20,21] and time-dependent nonlinear spectroscopy (e.g., four wave mixing[22]). Additional techniques have shown promise theoretically such as electron holography, where the movement of electrons can be directly imaged,[23] and stimulated X-ray Raman spectroscopy, where electron transfer can be monitored.[24] Each technique has advantages and disadvantages. X-ray ATA, for example, is in principle capable of measuring density changes around particular atoms in a molecule with high temporal resolution,[20] but this may require high populations of excited molecules to have sufficient contrast. HHS is an all-in-one process where an electron ionized from a molecule is used to probe the parent molecule, but this requires some way of relating the observed modulations in harmonics to the underlying dynamics. Often, the choice of the technique is system- and process-dependent.

Received: February 6, 2020
Published: May 29, 2020

https://dx.doi.org/10.1021/acs.jctc.0c00122
J. Chem. Theory Comput. 2020, 16, 4470−4478

Among these, X-ray ATA is especially promising for its relative simplicity, suitability for a range of molecules and solids, and excellent time resolution. In ATA, a pump pulse is used to excite the system, and the dynamics are probed via an attosecond probe pulse. The resulting modulations in the spectra as a function of the time delay (τ) between the two pulses encodes information about the electron dynamics initiated by the pump. The development of ultrafast X-ray sources, including high-harmonic generation(HHG)[20,25−27] and high-intensity pulses at free-electron lasers,[28−30] has led to isolated keV X-ray pulses with 2.5 as the duration for HHG methods[31] and a few hundred attoseconds for soft X-rays at X-ray-free electron lasers.[32] These pulses typically probe near-edge probe core-level transitions in a system (i.e., XANES), including both optical density changes and frequency shifts due to the motion of electrons.[23,33−35] What makes this technique especially powerful is that core-level transitions are highly localized in space around the absorbing atom. As such, modulations in a particular X-ray absorption feature can be directly related to the instantaneous electron density around that atom. There has been steady progress toward increasing the range of frequencies of attosecond X-ray sources. This has been realized for soft X-rays below 1.0 keV,[31] which spans the K-edge of carbon, nitrogen, oxygen, and fluorine. ATA, with heavier elements such as sulfur (K-edge at 2.6 keV), remains an ongoing challenge for X-ray sources.

Despite the advantages, transient absorption experiments can be difficult to interpret. Reconstructing the electron dynamics from modulations in the X-ray absorption often requires simulation of both the dynamics as well as the corresponding X-ray spectra. Much work has been done toward simulating the motion of electrons in molecules and solids. First-principles methods, in particular, offer a powerful tool for interpreting experiments without inputs from experiments. These all involve solving the time-dependent Schrödinger equation either via a direct numerical solution with tractable (e.g., one-electron molecules),[36] single active-electron models[37,38] or via a particular quantum chemistry approximation such as Hartree−Fock methods,[39] time-dependent multiconfigurational self-consistent field,[40] time-dependent coupled cluster,[41,42] and time-dependent density functional theory (TDDFT).[43] Among these, TDDFT is particularly useful, as it offers a good trade-off between accuracy and computational cost, and has been shown to adequately capture electronic dynamics and give accurate linear-response X-ray absorption spectra. TDDFT includes a many-body correlation via the exchange-correlation functional, which in practice is approximate.[44] Generally speaking, nonlocal methods such as hybrid DFT (mixture of HF and DFT) are known to give more accurate core-level and charge-transfer excitation energies, as well as improved electron dynamics. The TDDFT equations are generally solved in two ways. Linear-response (LR) TDDFT involves finding roots in the frequency-dependent response and gives spectra but cannot be used for electron dynamics.[45−49] Real-time (RT) TDDFT,[5,50−54] where the wave function/density matrix is propagated in time, allows for straightforward computation of the transient spectra following the interaction with the pump and probe lasers. One important caveat with TDDFT is that resonant excitation is poorly described due to the adiabatic (local-in-time) approximation for the DFT functional.

In contrast to dynamics, there has been far less work on simulating the corresponding attosecond transient X-ray spectra. Generally, some form of time-dependent Schrödinger equation is used, e.g., simulation of the electron dynamics in atoms using TR-XUV[37] and TR-XAS,[55] transient metallization of silica,[10,33] and exciton dynamics in magnesium oxide.[56] These methods, however, typically require parametrization, which can limit predictability. In terms of first-principles methods, TDDFT has been used to simulate the time-resolved XUV absorption of polycrystalline diamonds using coupled TDDFT−Maxwell's equations.[11] Recently, Nascimento and co-workers used linear-response TDDFT to show that single and double core-hole states can be used to probe valence electron dynamics.[57] Nevertheless, first-principles tools for computing explicit spectra as a function of the time delay between the pump and probe remain underdeveloped. These types of simulations are crucial for reconstructing the electron density movement in molecules from observed transient X-ray spectra.

To address this, in this paper, we present a methodology for using RT-TDDFT to directly compute X-ray ATA spectra in molecules, specifically for the case of measuring coherent electron dynamics. We interpret our results primarily in the language of electron density rather than states, i.e., how are X-ray modulations related to the instantaneous density surrounding the absorbing atom. We then use this method to simulate XTAS for carbon monoxide (CO), dioxygen (O_2), and 4-aminophenol following UV pump excitation, as well as for the benzene−tetracyanoethylene charge-transfer dimer.

2. METHODS

To simulate the transient spectra, we use real-time time-dependent density functional theory (RT-TDDFT) in a Gaussian basis set, as implemented in the NWChem software package.[51] This choice of basis allows for all-electron simulations (for the core states) and efficient evaluations of hybrid DFT functionals. The Born−Oppenheimer approximation is used throughout; given the short time scales (<2 fs) studied here, nuclear motion is not expected to have a significant effect on the dynamics,[58,59] but this remains an open question.[60] For all simulations, the von Neumann equation of motion was integrated using an exponential midpoint rule with a time step of Δt = 0.06 au = 1.45 as,

$$i\frac{d\mathbf{P}'}{dt} = [\mathbf{F}'\mathbf{P}' - \mathbf{P}'\mathbf{F}'] \tag{1}$$

where $\mathbf{P}'(t)$ and $\mathbf{F}'(t)$ are the density and Fock matrices in the canonical orthogonal basis (see ref 51 for details). This is sufficient to resolve the highest energy X-ray edges studied here (O K-edge around 520 eV). TDDFT is known to give spectra that are shifted from the experiment due to an incomplete description of the core-hole relaxation, primarily due to self-interaction errors.[61,62] TDDFT XANES spectra are often manually shifted to correct for this, but in this paper, we report unshifted spectra.

To bypass the issues with adiabatic (local-in-time) functionals for resonant excitations,[63,64] we instead emulate the state of the system following impulsive excitation by specifying the density distribution. As shown in Figure 1(a), this consists of specifying charges on particular regions of the molecule using constrained DFT,[65] resulting in a neutral charge-separated initial state. This allows for the simulation of time delays that occur after the pump has passed, i.e., how transient XAS can be used to probe field-free polarization-driven dynamics resulting from the pump. It may also be suitable

https://dx.doi.org/10.1021/acs.jctc.0c00122
J. Chem. Theory Comput. 2020, 16, 4470−4478

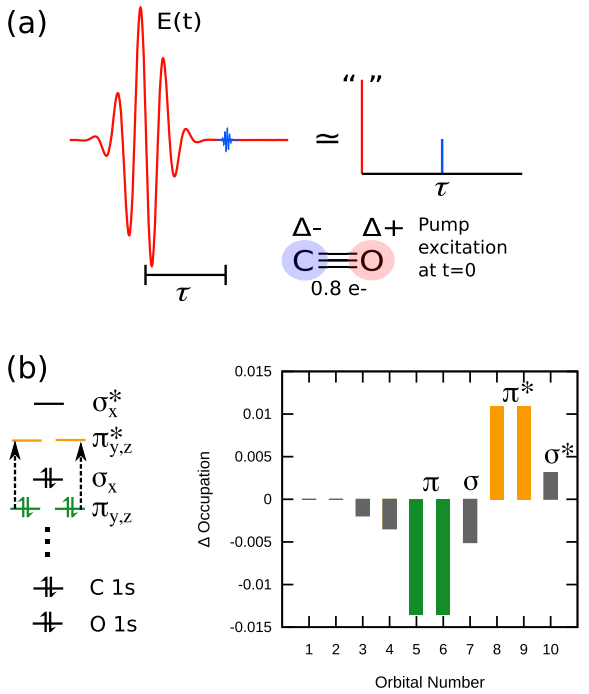

Figure 1. (a) UV/X-ray pump−probe scheme in carbon monoxide consisting of a "sudden" pump via constrained DFT followed by a time-delayed weak δ-function probe. (b) This pump primarily results in a partial population excitation from $\pi \rightarrow \pi^*$.

for cases where the pump laser is perpendicular to the direction of the electron dynamics. Since this method results in propagation starting from an excited-state density instead of the ground state, there is a formal TDDFT initial-state-dependence problem.[66] Nevertheless, this should have no practical consequences when using adiabatic exchange-correlation functionals, as done here. For each molecule, the specific density distribution was chosen to be reflective of the density change caused by a particular excitation (e.g., valence $\pi \rightarrow \pi^*$). For the molecules studied here, this corresponds to a value of $+\Delta$ on one end of the molecule and $-\Delta$ on the other. The actual effect of this "pump" can be assessed by comparing the molecular orbital populations and frequencies in the time-dependent dipole with those obtained from linear-response TDDFT. It is important to note that CDFT was designed to capture states involving charge transfer/deformation and is not well-suited for preparing an arbitrary intramolecular excitation.[67] Nevertheless, we observe that the results (dipole, OD modulation, and ω shifts) are all linear in the deviation of the atomic charges from the ground state (see Results and Supporting Information (SI) for details).

The probe was taken to be a δ-function delayed τ from $t = 0$ with an amplitude of 10^{-4} au, which corresponds to a perfectly broadband weak probe. In contrast to experiments, which typically probe a particular elemental edge with an attosecond X-ray pulse, our δ-function probe yields the entire X-ray spectrum. To compute the spectrum, we use the dipole strength function $S(\omega)$ from the Fourier transform (FT) of the time-dependent dipole moment. Although the CDFT pump results in very little core-level depopulation, in practice it does induce some weak high -frequency modes. These may occur in the X-ray absorption range with a polarization parallel to the dynamics (molecular axis). To compensate for this, we compute the difference dipole by subtracting out the dipole moment $\mu_p^0(t)$ from a simulation with the pump only. Formally, this is given by

$$\Delta\mu_p(\omega) = \int_0^\infty \mathrm{d}t\, [\mu_p(t) - \mu_p^0(t)]\mathrm{e}^{-(t-\tau)/k}\mathrm{e}^{i\omega t} \tag{2}$$

where τ is the time delay between the pump and the probe, k is the damping lifetime parameter, and $p = x, y, z$ denotes the polarization of the probe laser. This is conceptually similar to the subtraction of a "moving reference" density matrix.[68,69] Since the damping in the dipole starts at the time of the probe, all spectra generated for different τ values have the same phenomenological Lorentzian line widths. Note that this shifted damping assumes a vanishingly small time-dependent dipole before the probe, at least in the desired X-ray frequency range. In practice, subtraction of the pump-only dipole in eq 2 ensures this. The on-diagonal parts of the polarizability tensor $\alpha_{pp}(\omega)$ are then given by

$$\alpha_{pp}(\omega) = \frac{\Delta\mu_p(\omega)E_p^*(\omega)}{|E_p(\omega)|^2} \tag{3}$$

Finally, the dipole strength $S(\omega)$ is calculated from the imaginary parts of α:

$$S(\omega) = \frac{4\pi\omega}{3c}\mathrm{Im}[\alpha_{xx}(\omega) + \alpha_{yy}(\omega) + \alpha_{zz}(\omega)] \tag{4}$$

This single molecule quantity is related to the absorbance/optical density (OD) of a system through the number density of the system, but throughout this paper, we use OD and $\sigma(\omega)$ interchangeably. In practice, to reduce the simulation times required to reach convergence, the Fourier transforms in eq 3 are computed using Padé approximants.[70] As noted previously, our TDDFT XAS spectra are not shifted; thus, our absolute photon energies differ somewhat from experimental values.

3. RESULTS

In this section, we present results for three different systems: carbon moxoxide (CO), dioxygen (O_2), a benzene−tetracyanoethylene (TCNE) dimer ($C_6H_6\cdots C_6N_4$), and 4-aminophenol ($H_2NC_6H_4OH$). Diatomic molecules were chosen since they are straightforward to interpret the dynamics in terms of the dipole moment, i.e., which atom has excess electron density. CO is a simple case of a heteronuclear molecule, where charge oscillations may modulate O K-edge XAS. Carbon K-edge is not likely to be useful for complex molecules as the many nearly degenerate atoms yield difficult to interpret spectra. Thus, we do not focus on carbon XAS in this study. O_2 is chosen to be somewhat of a control, since it has two identical oxygen atoms, and thus, the XAS should not be able to distinguish between the carbon being on one versus the other. Benzene−tetracyanoethylene was chosen as an example of how to probe long-range charge-transfer excitations using XAS. Finally, aminophenol has two probe atoms (N, O) at opposite ends of the molecule and is a good example of how electron dynamics in polyatomic molecules can be probed with transient XAS.

3.1. Valence Dynamics in Carbon Monoxide. First, we present the result for an isolated carbon monoxide molecule. The geometry was optimized using the PBE0 hybrid functional and the def2-TZVP basis set. This functional and basis set were also used for all subsequent TDDFT simulations. To emulate a valence excitation, a neutral excited state was constructed by putting a $\Delta = 0.8$ positive charge on the carbon atom and a

https://dx.doi.org/10.1021/acs.jctc.0c00122
J. Chem. Theory Comput. 2020, 16, 4470−4478

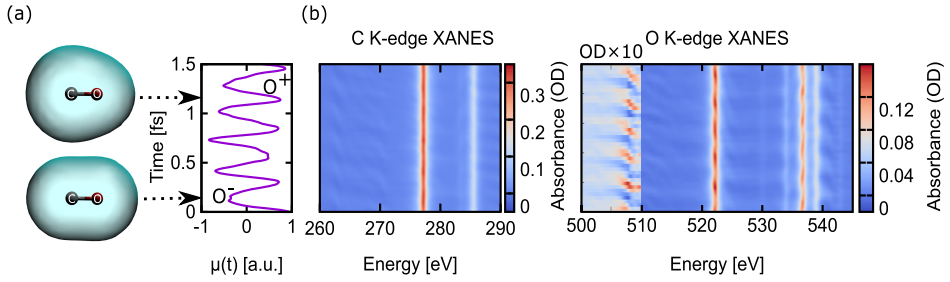

Figure 2. (a) The time-dependent dipole moment and density snapshots in CO following sudden excitation exhibits one dominant frequency, which corresponds to density oscillation between carbon and oxygen. (b) The transient XAS spectra show optical density and peak energy oscillations that are correlated with the dynamics. Additionally, pre-edge features appear (e.g., O K-edge at 508 eV) due to transitions to depopulated orbitals.

−0.8 charge on the oxygen atom via constrained DFT (CDFT) (see Figure 1(a)). The resulting orbital populations after this pump are shown in Figure 1(b). The pump essentially corresponds to a $\pi \rightarrow \pi^*$ excitation, with a slight $\sigma \rightarrow \sigma^*$ excitation, and virtually no C 1s orbital or O 1s orbital depopulation. The dynamics that result from this pump are dominated by a simple oscillation of charge between C and O with a period of 290 as, as shown by the dipole moment $\mu(t)$ in Figure 2(a). The $\pi \rightarrow \pi^*$ excitation character is further confirmed by comparing the frequency response of the dipole moment, computed via a Fourier transform, with the linear-response ultraviolet absorption spectrum for the unexcited molecule (see Supporting Information). The FT spectrum and the LR spectrum both have strong peaks at 14.3 eV, which confirms that this state is similar to what would result from a UV excitation.

The resulting C and O K-edge attosecond transient XAS spectra are shown in Figure 2(b). Due to a lack of decoherence in TDDFT, all the spectral features have the same artificial line width, which is dictated by the choice of the damping parameter (k = 1.2 fs) applied to the dipole before Fourier transforming. There are clear intensity and shift modulations with the same frequency as $\mu(t)$ for several peaks near the C and O K-edges. These are discussed in detail below. Additionally, there are pre-edge features, which are absent in the unpumped molecules (region scaled by ×10 in Figure 2(b)). These correspond to a 1s → π transition, i.e., transitions to a partially depopulated HOMO−1/HOMO−2 π-orbital. This feature oscillates with the same frequency as the dipole but has an evolving Fano line shape. In general, this is characteristic of a phase accumulated during interaction with a laser.[71] In our case this phase is indeterminate due the CDFT initial state, but is likely similar to the phase that would result from an impulsive excitation at t = 0. Pre-edge transitions such as this are useful experimentally, as they only appear in the pumped molecules and are therefore background-free. They are likely to be observed in any pumped molecule, but their intensities would depend on the specific transition dipoles to those states.

To understand the effect of oscillating charge on the TR-XAS, we compare the dipole moment to modulations in the simulated optical density and frequencies for specific peaks in these spectra. For simplicity, we only pick two peaks near the O K-edge and analyze the modulations in terms of the density around the O as well as the virtual orbital shapes. Figure 3(b) shows this for the bright peak near 522 eV (probe polarization perpendicular to the molecular axis), which is O 1s → π^* in character. When the excess electron density is around an

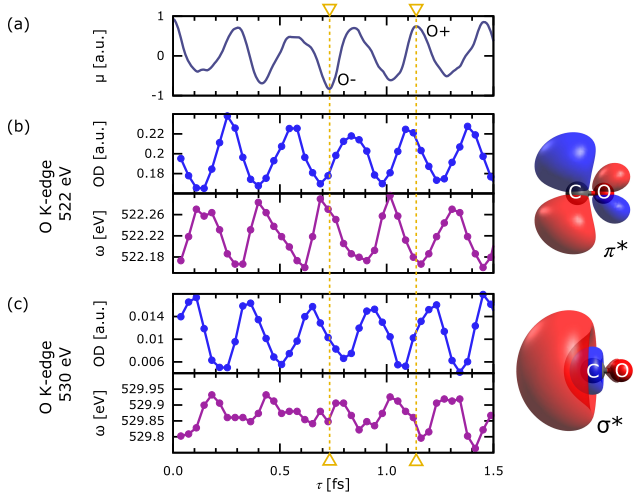

Figure 3. O K-edge modulations in CO. (a) The O K-edge 522 eV peak, which corresponds to a 1s→ π^* transition, shows an OD modulation of ±15% and a peak shift of ±0.05 eV. (b) The O K-edge peak at 530 eV, which involves a 1s→ σ^* transition, has an OD modulation of ±54% and a ω shift of ±0.07 eV. The modulations of these two spectra features have different delays with respect to the dynamics due to the different shapes of the virtual orbitals involved (see text).

oxygen atom (i.e., O is Δ^-), the optical density decreases by about 15%, and the peak blue shifts by ∼0.05 eV. Figure 3(c) shows the OD and ω for the dim peak at 530 eV (probe polarization parallel to the molecular axis), which is primarily O 1s → σ^*. This peak has a OD shift of ±54% and a ω shift of ±0.07 eV.

Additionally, there is a phase difference between these modulations and the dipole (e.g., see yellow lines on Figure 3). This can be explained in terms of the shape of the virtual orbitals involved. For the 522 eV peak, for example, the lobe of the π^* is centered slightly to the right of the O atom, whereas for the 530 eV peak the small lobe in the σ^* is left of the O atom. Since the OD is related to the overlap $|\langle 1s|z|\pi^*\rangle|$ and $|\langle 1s|z|\sigma^*\rangle|$, respectively, there is a shift in the OD with respect to the dipole moment. In general, these shifts complicate interpretation but may be useful for reconstructing density dynamics from the transient spectra.

Finally, we note that the particular values of the shifts reported here are specific to the choice of the CDFT initial charge Δ. To determine the effect of this "pump" strength on the transient shifts, we repeated the above simulations for Δ = 0.4. The resulting dipole, as well as OD and ω shifts, are almost

https://dx.doi.org/10.1021/acs.jctc.0c00122
J. Chem. Theory Comput. 2020, 16, 4470−4478

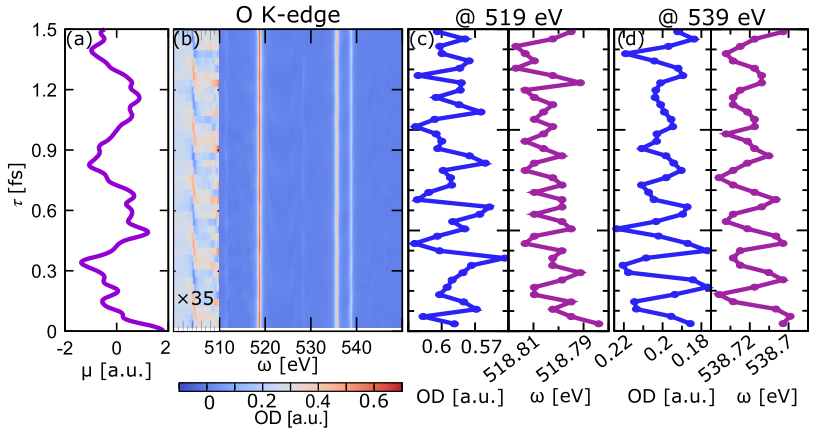

Figure 4. (a) Time-dependent dipole moment of O_2 following sudden CDFT excitation and (b) the resulting transient XAS spectrum. Due to the symmetry of the molecule, the modulation in OD and ω, as well as the pre-edge features, all oscillate at twice the frequency of the dynamics. (c) OD and ω modulations in O_2 for the 519 eV peak (β 1s → π^*) and (d) the modulations for the 539 eV ($\alpha\beta$ 1s → $n\pi^*$). The modulations occur at twice the frequency of the dynamics due to the symmetry of the molecule.

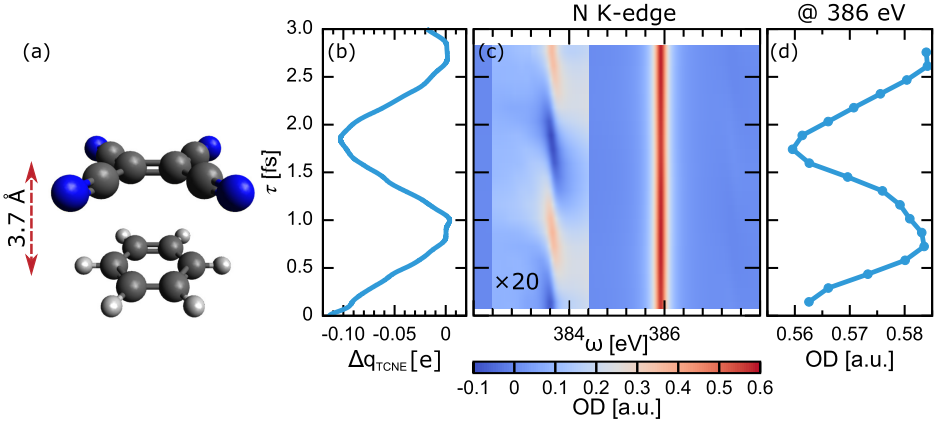

Figure 5. (a) Geometry of the benzene−tetracyanoethylene (TCNE) charge-transfer (CT) dimer. (b) Deviation of the time-dependent charge from the ground state for TCNE following a CDFT pump excitation that results in a CT excitation with a frequency of 2.2 eV. (c) The resulting transient XAS spectrum exhibits a weak pre-edge feature near 383.6 eV corresponding to a transition to the depopulated benzene-centered π orbital as well as a strong feature at 386 eV (N 1s → π^* on TCNE). (d) The N K-edge at the bright 386 eV peak shows a reduction in the optical density when the TCNE molecule has an extra electron density.

exactly 3.4 times less than the case of Δ = 0.8 (see SI for details). The proportionality of the dipole/shifts to the CDFT charge on each atom is linear in the deviation of atomic charge from the ground state. That is, for a homonuclear diatomic, Δ = 0.8 would give 2.0 times the response of Δ = 0.4. For CO, however, carbon is negative and oxygen positive in the ground state. The factor of 3.4 thus corresponds to carbon having an atomic charge of −0.23 for the ground state, which is similar to the computed Löwdin population of −0.25. In this paper, we picked intermediate values for Δ to avoid potential nonlinearities resulting from large deviations from the ground state. Due to the linearity of the response with respect to the "pump", the value of Δ can be loosely correlated with the experimental pump intensity.

3.2. Valence Dynamics in Dioxygen. Next, we present results for dioxygen (O_2), which consists of two equivalent oxygen atoms. This is a "control" example for the case of probing density motion in a molecule with two indistinguishable atoms, where time-resolved XAS would generally be considered unsuitable. To initiate the dynamics, a CDFT charge-separated density with a net charge of +0.8 on one oxygen and −0.8 on the other was used, with a triplet spin state (two unpaired α spins). This pump, which corresponds roughly to a β π → π^* transition, is not taken to reflect a superposition that could result from any particular laser pump but rather as a way of initiating the charge density oscillations dominated by a single frequency. Figure 4(a) shows the resulting dipole moment, which oscillates with a dominant low-frequency mode with a period of 0.6 fs as well as some higher frequency contributions. Figure 4(b) shows the corresponding transient O K-edge spectrum for a probe polarized perpendicular to the molecular axis. There is a clear pre-edge feature (zoomed), which corresponds to the O 1s → π β-spin transition. In contrast to CO, this modulation occurs at twice the frequency of the dynamics, which is expected given the two indistinguishable oxygen centers. For the post-edge peaks in the K-edge region of the O atom, we choose the peaks around 519 and 539 eV to reconstruct the low-frequency dynamics in the molecule. Both transitions involve light polarized perpendicular to the molecular axis. For the peak around 539 eV, which involves a O 1s orbital to a higher π^* orbital with both α and β spins, the double-frequency modulation in the OD and ω is clear. When the excess

https://dx.doi.org/10.1021/acs.jctc.0c00122
J. Chem. Theory Comput. 2020, 16, 4470−4478

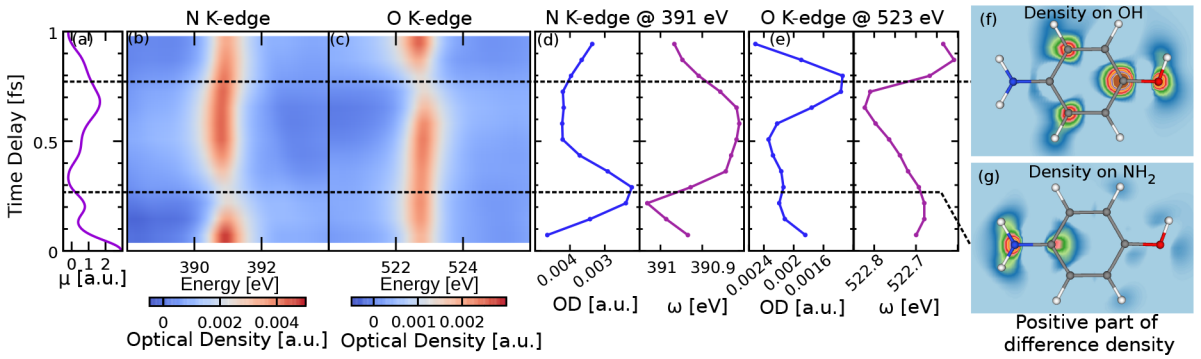

Figure 6. (a) Dipole moment in 4-aminophenol following the CDFT pump, and (b and c) the transient XAS for the N and O K-edges. (d) Transient N K-edge XAS shows an OD decrease of 42% and a ω blue-shift of 0.15 eV when nitrogen has the excess electron density. (e) Transient XAS for the O K-edge, which shows a decrease of 33% and a blue-shift of 0.1 eV when the oxygen has excess electron density. (f and g) Snapshots of the positive part of the difference density.

electron density is around the oxygen atom, the OD decreases by 12% and the peak blue shifts by about 0.015 eV.

For the peak at 519 eV, which is related to the O 1s → π^* β spin transition, roughly speaking there is a modulation in the OD at double the frequency. There is no obvious correlation, however, between the dynamics and the peak energy. This is likely a consequence of the open-shell (triplet) state of the molecule and can be understood as follows. Although this transition probes the β π^*, these orbital energies are coupled to the α orbitals via the total density. Here, the dynamics involve both the pump-populated singlet β π^* population as well as the pump-depopulated triplet α π^* population. Due to the use of an instantaneous pump, these are out-of-phase with each other, and there is no clear correlation between the edge energy and the dipole moment. Performing a simulation with an explicit pump may remedy this, but it is likely that correlating edge shifts with density dynamics will be challenging for pumped open-shell systems.

3.3. Charge-Transfer Excitation in a Benzene−TCNE Dimer. Next, we present results for a molecular dimer consisting of a benzene molecule separated from a tetracyanoethylene (TCNE) molecule in a coplanar π-stacked configuration. This is a prototypical charge-transfer (CT) complex where the TCNE acts as an electron acceptor in a excitation involving a π electron on the benzene going to a π^* orbtial on the TCNE. As CDFT is known to work better for CT states than for intramolecular excitations,[67] we use this example to verify the validity of CDFT for an initial state and as an example of probing CT excitations with TXAS. For the geometry, we use the previously reported case[72] of benzene separated from TCNE by 3.7 Å (Figure 5(a)). To be consistent with this study, we use the cc-pVDZ basis set and the B3LYP functional. It is well-known that global hybrid functionals such as B3LYP underestimate the CT excitation energies,[73] which can be remedied by using a (tuned) range-separated functional.[72] In this paper, however, the emphasis is on creating and probing a particular known state rather than getting accurate energies.

Since the goal is to create a superposition of only the ground and one CT state, we initialized the system at $t = 0$ with a net negative charge of $\Delta q^{\mathrm{TCNE}}(0)$, with respect to the ground state, and a corresponding positive charge on the benzene. To determine what value of the initial charge to choose, we computed the time-dependent deviation of the charge on TCNE from the ground state for a range of initial charge values:

$$\Delta q^{\mathrm{TCNE}}(t) = q^{\mathrm{TCNE}}(t) - q_{\mathrm{GS}}^{\mathrm{TCNE}} \tag{5}$$

We use a Mulliken scheme for the charges, which is well-defined for the case of two separate molecules with a balanced basis set. If appropriately chosen, the dynamics should consist of an oscillation between TCNE^-−$\mathrm{benzene}^+$ and TCNE−benzene that has the same frequency as the corresponding linear-response TDDFT excitation. As shown in Figure 5(b), we found that a CDFT value of $\Delta = -0.17$ e ($\Delta q^{\mathrm{TCNE}}(0) = -0.12$ e) gave charge dynamics that oscillate between the neutral and partially negatively charged TCNE. Using this value of Δ gave a CT frequency for the transition of about 2.2 eV, which is in good agreement with the previously reported LR value of 2.1 eV.[72] Smaller or larger Δ resulted in oscillations that do not return to the charge of the ground-state TCNE ($\Delta q^{\mathrm{TCNE}} = 0$) but still gave excitation frequencies close to 2.2 eV, at least in the vicinity of 0.17 e. In terms of orbtial populations, this pump moves about 2% of an electron from the HOMO (benzene π) to the LUMO (TCNE π^*).

Figure 5(c) shows the resulting TR-XAS spectrum for the N K-edge for the case of a z-polarized probe, which points along the direction of the π-stacked system. Since TCNE contains four equivalent N atoms, the transient N K-edge spectra are expected to act as a probe of the instantaneous charge of the TCNE molecule. Here, we used a damping parameter $k = 200$ au = 4.8 fs for broadening the peaks. There is a weak pre-edge feature at around 384 eV that oscillates with the CT frequency. This arises from a N 1s → π transition, which is absent in the unexcited system. Due to the poor overlap of the N 1s orbital on the TCNE molecule and the π orbital on the benzene, this peak has a low oscillator strength. In general, such features might be difficult to observe experimentally for intramolecular CT processes due to this minimal overlap. The peak at about 386 eV in Figure 5(c) is related to a N 1s→ π^* transition, both of which are located on the TCNE molecule. Looking at the optical density of this peak as a function of the time delay (Figure 5(d)) shows that when the extra electron density is on the TCNE, the OD decreases by about 3% compared to when the TCNE is neutral. Although qualitatively similar to the CO case where the OD decreases with an increasing electron density around the probe atom, here, the OD reduction with density is significantly less pronounced. This is likely a consequence of the spatial extent of the CT excitation. At the

https://dx.doi.org/10.1021/acs.jctc.0c00122
J. Chem. Theory Comput. 2020, 16, 4470−4478

times when the TCNE molecule is negatively charged with respect to the ground state, the extra density is delocalized across the π^* system, primarily above/below the carbon atoms and to a lesser extent around the four nitrogen atoms. Since the XAS is a local probe of the density around each N atom, the resulting modulation of the K-edge OD is rather subtle. Similarly, only a minor edge shift is observed here (±0.002 eV), which is well below the experimental resolution. This may limit the utility of attosecond XAS for measuring this type of excitation.

3.4. Valence Dynamics in 4-Aminophenol. Finally, we present transient XAS for 4-aminophenol, which is a prototypical example of a molecule with two distinct atoms (O and N) that can be probed with XANES. Carbon can in principle also be probed, but the six nearly degenerate carbon atoms make it difficult to interpret the C K-edge spectrum. For the sudden excitation here, we apply 0.3 e^- on NH_2 and 0.3 e^+ on OH at $t = 0$. This pump roughly corresponds to a $\pi \rightarrow \pi^*$ excitation. The polarization of the probe is chosen to be perpendicular to the plane of the phenyl ring.

The resulting dipole shows a quasi-single frequency, as shown in Figure 6(a). Snapshots of the positive part of the difference density at two extremes of the oscillation are shown in panels (f) and (g), ranging from 0 to 0.01 au. These were obtained by subtracting the ground-state density $\rho_0(r)$ from the time-dependent one:

$$\Delta\rho(\boldsymbol{r}, t) = \rho(\boldsymbol{r}, t) - \rho_0(\boldsymbol{r}) \tag{6}$$

At one extreme of the oscillation (f), the extra electron density is around the ring and the OH group. For the other extreme (g), the excess electron density is mostly on the NH_2 group. Panel (b) shows the corresponding XAS for the lowest N and O K-edge features. For the N K-edge peak at 391 eV, when the charge density is around the N atom, the absorbance is decreased by 42% and blue-shifted by 0.15 eV. For the O K-edge peak at 523 eV, the OD decreases by around 33%, and the peak blue shifts by about 0.1 eV. Taken as a whole, these results demonstrate that the N and O K-edges can act as two separate but complementary probes of the electron density, with the OD modulations being related to the dynamics in a straightforward way. These modulations are substantially more pronounced than the CO and O_2 cases. This is likely a consequence of the more localized time-dependent charge on the −OH and $-NH_2$ groups as compared to CO.

4. CONCLUSIONS

In conclusion, we have presented a methodology for using real-time TDDFT to compute attosecond X-ray transient absorption in molecules. Using the relatively simple cases of UV-excited CO, O_2, and aminophenol, as well as a benzene−TCNE charge-transfer dimer, our results show that, in principle, the instantaneous electron density around a particular atom results in both optical density modulations and frequency shifts. Qualitatively, the OD decreases and the frequency blue-shifts with increasing electron density around the probe atom. For the CO molecule, for example, OD shifts for the O K-edge are approximately 15% and ω shifts are on the order of 0.05 eV for excited populations of 2%. For the larger polyatomic molecule aminophenol, these shifts were approximately 42% in the OD and 0.15 eV for the edge energy of the N K-edge for populations of 3%. For the case of a charge-transfer complex (benzene−tetracynaoethylene) the OD modulations are significantly less pronounced, due primarily to a large delocalization of the extra electron density across the TCNE molecule.

These OD modulations can be understood in two ways. In a density-based interpretation, the increased charge around an atom reduces the transition probability for an inner-shell probe excitation from that atom, as the excitation is somewhat local to the region around the absorbing atom. Alternatively, this can be viewed as an orbital population effect, where the OD corresponding to a particular orbital is reduced with increasing population. In some cases, these shifts were delayed with respect to the dynamics (dipole moment), which is likely due to different overlaps of the states involved. We observe that these shifts are quite small (on the order of 0.1 eV or less) and may be below the resolution of current X-ray facilities. Additionally, we observe pre-edge features arising from transitions to depopulated orbitals. Since these only occur in excited molecules and these transitions are at frequencies outside of the ground-state absorption, they may be advantageous to focus experimentally on these "background-free" features.

Due to the use of a CDFT initial state in these simulations and the ambiguous choice of an initial charge separation, it is difficult to draw specific conclusions about the shifts that might be observed in an experiment. In the future, alternative methods for constructing an initial state are likely required to get more predictive attosecond XTA spectra. Nevertheless, our results show qualitatively that the greater the localization of the excess electron density around a "probe" atom, the greater the change in the OD and ω shift. In aminophenol, the excess density is localized on the amine and hydroxyl groups, giving high-OD contrast and shifts. In benzene−TCNE, the excess density is completely delocalized across the TCNE molecule, with each of the four probe N atoms getting only a small fraction, resulting in small OD modulations. Overall, this suggests that transient XAS is best suited to probing dynamics where there are localized density changes, such as in attosecond charge migration.[1,6,74]

Going forward, due to the complexity of transient X-ray spectra, first-principles simulations like these will likely prove critical for interpreting experiments and for proposing future targets for X-ray free-electron laser studies, such as impulsive inner-shell ionization-triggered dynamics in polyatomic molecules. Additionally, these experiments will be valuable for validating the accuracy of simulation methodologies.

■ ASSOCIATED CONTENT

Supporting Information

The Supporting Information is available free of charge at https://pubs.acs.org/doi/10.1021/acs.jctc.0c00122.

The molecular orbital diagram and ground-state XANES for CO, an analysis of the state created by the pump, the effect of the initial state on the dynamics and transient spectra, the optimized molecular geometries, and Table S1 and Figures S1−S4 (PDF)

■ AUTHOR INFORMATION

Corresponding Author

Kenneth Lopata − *Department of Chemistry and Center for Computation and Technology, Louisiana State University, Baton Rouge, Louisiana 70803, United States;* orcid.org/0000-0002-9141-684X; Email: klopata@lsu.edu

https://dx.doi.org/10.1021/acs.jctc.0c00122
J. Chem. Theory Comput. 2020, 16, 4470−4478

Author

Min Chen − *Department of Chemistry, Louisiana State University, Baton Rouge, Louisiana 70803, United States*

Complete contact information is available at: https://pubs.acs.org/10.1021/acs.jctc.0c00122

Notes

The authors declare no competing financial interest.

■ ACKNOWLEDGMENTS

This work was supported by the U.S. Department of Energy, Office of Science, Basic Energy Sciences, Atomic, Molecular and Optical Sciences program, under Contract Number DE-SC0017868. Conversations with James Cryan, Kenneth Schafer, and Mette Gaarde are gratefully acknowledged.

■ REFERENCES

(1) Kraus, P. M.; et al. Measurement and laser control of attosecond charge migration in ionized iodoacetylene. *Science* **2015**, *350*, 790−795.

(2) Goulielmakis, E.; et al. Real-time observation of valence electron motion. *Nature* **2010**, *466*, 739.

(3) Kuleff, A. I.; Kryzhevoi, N. V.; Pernpointner, M.; Cederbaum, L. S. Core ionization initiates subfemtosecond charge migration in the valence shell of molecules. *Phys. Rev. Lett.* **2016**, *117*, 093002.

(4) Yuan, K.-J.; Bandrauk, A. D. Probing Attosecond Electron Coherence in Molecular Charge Migration by Ultrafast X-Ray Photoelectron Imaging. *Appl. Sci.* **2019**, *9*, 1941.

(5) Schelter, I.; Kümmel, S. Accurate Evaluation of Real-Time Density Functional Theory Providing Access to Challenging Electron Dynamics. *J. Chem. Theory Comput.* **2018**, *14*, 1910−1927.

(6) Bruner, A.; Hernandez, S.; Mauger, F.; Abanador, P. M.; LaMaster, D. J.; Gaarde, M. B.; Schafer, K. J.; Lopata, K. Attosecond charge migration with TDDFT: Accurate dynamics from a well-defined initial state. *J. Phys. Chem. Lett.* **2017**, *8*, 3991−3996.

(7) Schriber, J. B.; Evangelista, F. A. Time dependent adaptive configuration interaction applied to attosecond charge migration. *J. Chem. Phys.* **2019**, *151*, 171102.

(8) Perfetto, E.; Trabattoni, A.; Calegari, F.; Nisoli, M.; Marini, A.; Stefanucci, G. Ultrafast Quantum Interference in the Charge Migration of Tryptophan. *J. Phys. Chem. Lett.* **2020**, *11*, 891.

(9) Schultze, M.; et al. Attosecond band-gap dynamics in silicon. *Science* **2014**, *346*, 1348−1352.

(10) Krausz, F.; Stockman, M. I. Attosecond metrology: from electron capture to future signal processing. *Nat. Photonics* **2014**, *8*, 205.

(11) Lucchini, M.; Sato, S. A.; Ludwig, A.; Herrmann, J.; Volkov, M.; Kasmi, L.; Shinohara, Y.; Yabana, K.; Gallmann, L.; Keller, U. Attosecond dynamical Franz-Keldysh effect in polycrystalline diamond. *Science* **2016**, *353*, 916−919.

(12) Andrade, X.; Hamel, S.; Correa, A. A. Negative differential conductivity in liquid aluminum from real-time quantum simulations. *Eur. Phys. J. B* **2018**, *91*, 229.

(13) Hentschel, M.; Kienberger, R.; Spielmann, C.; Reider, G. A.; Milosevic, N.; Brabec, T.; Corkum, P.; Heinzmann, U.; Drescher, M.; Krausz, F. Attosecond metrology. *Nature* **2001**, *414*, 509.

(14) Krausz, F.; Ivanov, M. Attosecond physics. *Rev. Mod. Phys.* **2009**, *81*, 163.

(15) Shiner, A.; Schmidt, B.; Trallero-Herrero, C.; Wörner, H. J.; Patchkovskii, S.; Corkum, P. B.; Kieffer, J.; Légaré, F.; Villeneuve, D. Probing collective multi-electron dynamics in xenon with high-harmonic spectroscopy. *Nat. Phys.* **2011**, *7*, 464.

(16) Wörner, H. J.; et al. Conical intersection dynamics in NO2 probed by homodyne high-harmonic spectroscopy. *Science* **2011**, *334*, 208−212.

(17) Cavalieri, A. L.; et al. Attosecond spectroscopy in condensed matter. *Nature* **2007**, *449*, 1029.

(18) Cousin, S. L.; Di Palo, N.; Buades, B.; Teichmann, S. M.; Reduzzi, M.; Devetta, M.; Kheifets, A.; Sansone, G.; Biegert, J. Attosecond streaking in the water window: A new regime of attosecond pulse characterization. *Phys. Rev. X* **2017**, *7*, 041030.

(19) Remetter, T.; et al. Attosecond electron wave packet interferometry. *Nat. Phys.* **2006**, *2*, 323.

(20) Geneaux, R.; Marroux, H. J.; Guggenmos, A.; Neumark, D. M.; Leone, S. R. Transient absorption spectroscopy using high harmonic generation: a review of ultrafast X-ray dynamics in molecules and solids. *Philos. Trans. R. Soc., A* **2019**, *377*, 20170463.

(21) Driver, T.; Li, S.; Champenois, E. G.; Duris, J.; Ratner, D.; Lane, T. J.; Rosenberger, P.; Al-Haddad, A.; Averbukh, V.; Barnard, T.; Berrah, N.; Bostedt, C.; Bucksbaum, P. H.; Coffee, R.; DiMauro, L. F.; Fang, L.; Garratt, D.; Gatton, A.; Guo, Z.; Hartmann, G.; Haxton, D.; Helml, W.; Huang, Z.; LaForge, A.; Kamalov, A.; Kling, M. F.; Knurr, J.; Lin, M.-F.; Lutman, A. A.; MacArthur, J. P.; Marangos, J. P.; Nantel, M.; Natan, A.; Obaid, R.; O'Neal, J. T.; Shivaram, N. H.; Schori, A.; Walter, P.; Li Wang, A.; Wolf, T. J. A.; Marinelli, A.; Cryan, J. P. Attosecond transient absorption spooktroscopy: a ghost imaging approach to ultrafast absorption spectroscopy. *Phys. Chem. Chem. Phys.* **2020**, *22*, 2704.

(22) Materny, A.; Chen, T.; Schmitt, M.; Siebert, T.; Vierheilig, A.; Engel, V.; Kiefer, W. Wave packet dynamics in different electronic states investigated by femtosecond time-resolved four-wave-mixing spectroscopy. *Appl. Phys. B: Lasers Opt.* **2000**, *71*, 299−317.

(23) He, M.; Li, Y.; Zhou, Y.; Li, M.; Cao, W.; Lu, P. Direct visualization of valence electron motion using strong-field photo-electron holography. *Phys. Rev. Lett.* **2018**, *120*, 133204.

(24) Zhang, Y.; Biggs, J. D.; Govind, N.; Mukamel, S. Monitoring long-range electron transfer pathways in proteins by stimulated attosecond broadband x-ray Raman spectroscopy. *J. Phys. Chem. Lett.* **2014**, *5*, 3656−3661.

(25) Canova, F.; Poletto, L. *Optical Technologies for Extreme-Ultraviolet and Soft X-ray Coherent Sources*; Springer, 2015.

(26) Ferray, M.; L'Huillier, A.; Li, X.; Lompre, L.; Mainfray, G.; Manus, C. Multiple-harmonic conversion of 1064 nm radiation in rare gases. *J. Phys. B: At., Mol. Opt. Phys.* **1988**, *21*, L31.

(27) Chini, M.; et al. Coherent phase-matched VUV generation by field-controlled bound states. *Nat. Photonics* **2014**, *8*, 437.

(28) McNeil, B. W.; Thompson, N. R. X-ray free-electron lasers. *Nat. Photonics* **2010**, *4*, 814.

(29) Seddon, E.; et al. Short-wavelength free-electron laser sources and science: a review. *Rep. Prog. Phys.* **2017**, *80*, 115901.

(30) Pellegrini, C. X-ray free-electron lasers: from dreams to reality. *Phys. Scr.* **2016**, *T169*, 014004.

(31) Popmintchev, T.; et al. Bright coherent ultrahigh harmonics in the keV x-ray regime from mid-infrared femtosecond lasers. *Science* **2012**, *336*, 1287−1291.

(32) Coffee, R. N.; Cryan, J. P.; Duris, J.; Helml, W.; Li, S.; Marinelli, A. Development of ultrafast capabilities for X-ray free-electron lasers at the linac coherent light source. *Philos. Trans. R. Soc., A* **2019**, *377*, 20180386.

(33) Schultze, M.; et al. Controlling dielectrics with the electric field of light. *Nature* **2013**, *493*, 75.

(34) Attar, A. R.; Piticco, L.; Leone, S. R. Core-to-valence spectroscopic detection of the CH2Br radical and element-specific femtosecond photodissociation dynamics of CH2IBr. *J. Chem. Phys.* **2014**, *141*, 164308.

(35) Kübel, M.; Dube, Z.; Naumov, A. Y.; Villeneuve, D. M.; Corkum, P. B.; Staudte, A. Spatiotemporal imaging of valence electron motion. *Nat. Commun.* **2019**, *10*, 1042.

(36) Bandrauk, A. D.; Chelkowski, S.; Nguyen, H. S. Attosecond localization of electrons in molecules. *Int. J. Quantum Chem.* **2004**, *100*, 834−844.

(37) Wu, M.; Chen, S.; Camp, S.; Schafer, K. J.; Gaarde, M. B. Theory of strong-field attosecond transient absorption. *J. Phys. B: At., Mol. Opt. Phys.* **2016**, *49*, 062003.

(38) Fidler, A. P.; Camp, S. J.; Warrick, E. R.; Bloch, E.; Marroux, H. J.; Neumark, D. M.; Schafer, K. J.; Gaarde, M. B.; Leone, S. R.

Nonlinear XUV signal generation probed by transient grating spectroscopy with attosecond pulses. *Nat. Commun.* **2019**, *10*, 1−8.
(39) Kulander, K. C. Time-dependent Hartree-Fock theory of multiphoton ionization: Helium. *Phys. Rev. A: At., Mol., Opt. Phys.* **1987**, *36*, 2726.
(40) Meyer, H.-D.; Manthe, U.; Cederbaum, L. S. The multi-configurational time-dependent Hartree approach. *Chem. Phys. Lett.* **1990**, *165*, 73−78.
(41) Sato, T.; Pathak, H.; Orimo, Y.; Ishikawa, K. L. Communication: Time-dependent optimized coupled-cluster method for multielectron dynamics. *J. Chem. Phys.* **2018**, *148*, 051101.
(42) Huber, C.; Klamroth, T. Explicitly time-dependent coupled cluster singles doubles calculations of laser-driven many-electron dynamics. *J. Chem. Phys.* **2011**, *134*, 054113.
(43) Bauernschmitt, R.; Ahlrichs, R. Treatment of electronic excitations within the adiabatic approximation of time dependent density functional theory. *Chem. Phys. Lett.* **1996**, *256*, 454−464.
(44) Gross, E.; Kohn, W. *Advances in quantum chemistry*; Elsevier, 1990; Vol. *21*, pp 255−291.
(45) Gross, E.; Kohn, W. Local density-functional theory of frequency-dependent linear response. *Phys. Rev. Lett.* **1985**, *55*, 2850.
(46) Casida, M. E. Time-Dependent Density Functional Response Theory for Molecules. In *Recent Advances in Density Functional Methods*; Chong, D., Ed.; World Scientific, 1995.
(47) Liang, W.; Fischer, S. A.; Frisch, M. J.; Li, X. Energy-specific linear response TDHF/TDDFT for calculating high-energy excited states. *J. Chem. Theory Comput.* **2011**, *7*, 3540−3547.
(48) Stetina, T. F.; Kasper, J. M.; Li, X. Modeling L2, 3-edge X-ray absorption spectroscopy with linear response exact two-component relativistic time-dependent density functional theory. *J. Chem. Phys.* **2019**, *150*, 234103.
(49) Nenov, A.; Segatta, F.; Bruner, A.; Mukamel, S.; Garavelli, M. X-ray linear and non-linear spectroscopy of the ESCA molecule. *J. Chem. Phys.* **2019**, *151*, 114110.
(50) Yabana, K.; Bertsch, G. Time-dependent local-density approximation in real time. *Phys. Rev. B: Condens. Matter Mater. Phys.* **1996**, *54*, 4484.
(51) Lopata, K.; Govind, N. Modeling fast electron dynamics with real-time time-dependent density functional theory: application to small molecules and chromophores. *J. Chem. Theory Comput.* **2011**, *7*, 1344−1355.
(52) Andrade, X.; et al. Real-space grids and the Octopus code as tools for the development of new simulation approaches for electronic systems. *Phys. Chem. Chem. Phys.* **2015**, *17*, 31371−31396.
(53) Goings, J. J.; Kasper, J. M.; Egidi, F.; Sun, S.; Li, X. Real time propagation of the exact two component time-dependent density functional theory. *J. Chem. Phys.* **2016**, *145*, 104107.
(54) Fernando, R. G.; Balhoff, M. C.; Lopata, K. X-ray absorption in insulators with non-Hermitian real-time time-dependent density functional theory. *J. Chem. Theory Comput.* **2015**, *11*, 646−654.
(55) Chew, A.; Douguet, N.; Cariker, C.; Li, J.; Lindroth, E.; Ren, X.; Yin, Y.; Argenti, L.; Hill, W. T., III; Chang, Z. Attosecond transient absorption spectrum of argon at the L 2, 3 edge. *Phys. Rev. A: At., Mol., Opt. Phys.* **2018**, *97*, 031407.
(56) Géneaux, R. et al. Attosecond time-domain measurement of core-excitonic decay in magnesium oxide. *arXiv preprint* 2019, arXiv:1912.12266.
(57) Nascimento, D. R.; Zhang, Y.; Bergmann, U.; Govind, N. Near-Edge X-ray Absorption Fine Structure Spectroscopy of Heteroatomic Core-Holestates as a Probe for Nearly Indistinguishable Chemical Environments. *J. Phys. Chem. Lett.* **2020**, *11*, 556.
(58) Despré, V.; Marciniak, A.; Loriot, V.; Galbraith, M.; Rouzée, A.; Vrakking, M.; Lépine, F.; Kuleff, A. Attosecond hole migration in benzene molecules surviving nuclear motion. *J. Phys. Chem. Lett.* **2015**, *6*, 426−431.
(59) Lara-Astiaso, M.; et al. Attosecond pump−probe spectroscopy of charge dynamics in tryptophan. *J. Phys. Chem. Lett.* **2018**, *9*, 4570−4577.
(60) Palacios, A.; Martín, F. The quantum chemistry of attosecond molecular science. *WIREs Comput. Mol. Sci.* **2020**, *10*, e1430.
(61) Besley, N. A.; Peach, M. J.; Tozer, D. J. Time-dependent density functional theory calculations of near-edge X-ray absorption fine structure with short-range corrected functionals. *Phys. Chem. Chem. Phys.* **2009**, *11*, 10350−10358.
(62) Derricotte, W. D.; Evangelista, F. A. Simulation of X-ray absorption spectra with orthogonality constrained density functional theory. *Phys. Chem. Chem. Phys.* **2015**, *17*, 14360−14374.
(63) Fuks, J. I.; Luo, K.; Sandoval, E. D.; Maitra, N. T. Time-resolved spectroscopy in time-dependent density functional theory: An exact condition. *Phys. Rev. Lett.* **2015**, *114*, 183002.
(64) Provorse, M. R.; Habenicht, B. F.; Isborn, C. M. Peak-shifting in real-time time-dependent density functional theory. *J. Chem. Theory Comput.* **2015**, *11*, 4791−4802.
(65) Wu, Q.; Van Voorhis, T. Direct optimization method to study constrained systems within density-functional theory. *Phys. Rev. A: At., Mol., Opt. Phys.* **2005**, *72*, 024502.
(66) Runge, E.; Gross, E. K. Density-functional theory for time-dependent systems. *Phys. Rev. Lett.* **1984**, *52*, 997.
(67) Kaduk, B.; Kowalczyk, T.; Van Voorhis, T. Constrained density functional theory. *Chem. Rev.* **2012**, *112*, 321−370.
(68) Fischer, S. A.; Cramer, C. J.; Govind, N. Excited state absorption from real-time time-dependent density functional theory. *J. Chem. Theory Comput.* **2015**, *11*, 4294−4303.
(69) Fischer, S. A.; Cramer, C. J.; Govind, N. Excited-state absorption from real-time time-dependent density functional theory: optical limiting in Zinc phthalocyanine. *J. Phys. Chem. Lett.* **2016**, *7*, 1387−1391.
(70) Bruner, A.; LaMaster, D.; Lopata, K. Accelerated broadband spectra using transition dipole decomposition and Padé approximants. *J. Chem. Theory Comput.* **2016**, *12*, 3741−3750.
(71) Ott, C.; Kaldun, A.; Raith, P.; Meyer, K.; Laux, M.; Evers, J.; Keitel, C. H.; Greene, C. H.; Pfeifer, T. Lorentz meets Fano in spectral line shapes: a universal phase and its laser control. *Science* **2013**, *340*, 716−720.
(72) Stein, T.; Kronik, L.; Baer, R. Reliable prediction of charge transfer excitations in molecular complexes using time-dependent density functional theory. *J. Am. Chem. Soc.* **2009**, *131*, 2818−2820.
(73) Autschbach, J. Charge-Transfer Excitations and Time-Dependent Density Functional Theory: Problems and Some Proposed Solutions. *ChemPhysChem* **2009**, *10*, 1757−1760.
(74) Kuleff, A. I.; Lunnemann, S.; Cederbaum, L. S. Ultrafast charge migration following valence ionization of 4-methylphenol: jumping over the aromatic ring. *J. Phys. Chem. A* **2010**, *114*, 8676−8679.

https://dx.doi.org/10.1021/acs.jctc.0c00122
J. Chem. Theory Comput. 2020, 16, 4470−4478